Comparison of Airborne Hyperspectral Data and EO-1 Hyperion for Mineral Mapping

Fred A. Kruse, *Member, IEEE*, Joseph W. Boardman, and Jonathan F. Huntington

***Abstract*—Airborne hyperspectral data have been available to researchers since the early 1980s and their use for geologic applications is well documented. The launch of the National Aeronautics and Space Administration Earth Observing 1 Hyperion sensor in November 2000 marked the establishment of a test bed for spaceborne hyperspectral capabilities. Hyperion covers the 0.4–2.5-μm range with 242 spectral bands at approximately 10-nm spectral resolution and 30-m spatial resolution. Analytical Imaging and Geophysics LLC and the Commonwealth Scientific and Industrial Research Organisation have been involved in efforts to evaluate, validate, and demonstrate Hyperions's utility for geologic mapping in a variety of sites in the United States and around the world. Initial results over several sites with established ground truth and years of airborne hyperspectral data show that Hyperion data from the shortwave infrared spectrometer can be used to produce useful geologic (mineralogic) information. Minerals mapped include carbonates, chlorite, epidote, kaolinite, alunite, buddingtonite, muscovite, hydrothermal silica, and zeolite. Hyperion data collected under optimum conditions (summer season, bright targets, well-exposed geology) indicate that Hyperion data meet prelaunch specifications and allow subtle distinctions such as determining the difference between calcite and dolomite and mapping solid solution differences in micas caused by substitution in octahedral molecular sites. Comparison of airborne hyperspectral data [from the Airborne Visible/Infrared Imaging Spectrometer (AVIRIS)] to the Hyperion data establishes that Hyperion provides similar basic mineralogic information, with the principal limitation being limited mapping of fine spectral detail under less-than-optimum acquisition conditions (winter season, dark targets) based on lower signal-to-noise ratios. Case histories demonstrate the analysis methodologies and level of information available from the Hyperion data. They also show the viability of Hyperion as a means of extending hyperspectral mineral mapping to areas not accessible to aircraft sensors. The analysis results demonstrate that spaceborne hyperspectral sensors can produce useful mineralogic information, but also indicate that SNR improvements are required for future spaceborne sensors to allow the same level of mapping that is currently possible from airborne sensors such as AVIRIS.**

***Index Terms*—Cuprite, Nevada, Death Valley, California, Earth Observing 1 (EO-1) Hyperion, hyperspectral imagery (HSI), hyperspectral imaging, mineral mapping.**

Manuscript received May 23, 2002; revised January 27, 2003. This research was supported in part by the National Aeronautics and Space Administration under Grant NCC5-495. Additional financial support was provided by Analytical Imaging and Geophysics LLC internal research and development funds.

F. A. Kruse and J. W. Boardman are with Analytical Imaging and Geophysics LLC (AIG), Boulder, CO 80303 USA (e-mail: kruse@aigllc.com).

J. F. Huntington is with the Division of Exploration and Mining, Commonwealth Scientific and Industrial Research Organisation (CSIRO), North Ryde, NSW, Australia, 2113.

Digital Object Identifier 10.1109/TGRS.2003.812908

I. Introduction

IMAGING spectrometry data or hyperspectral imagery (HSI) acquired using airborne systems have been used in the geologic community since the early 1980's and represent a mature technology. The solar spectral range 0.4–2.5 μm provides abundant information about many important earth-surface minerals [1]. In particular, the 2.0–2.5-μm shortwave infrared (SWIR) spectral range covers spectral features of hydroxyl-bearing minerals, sulfates, and carbonates common to many geologic units and hydrothermal alteration assemblages. Spectrally distinct minerals such as kaolinite, alunite, muscovite, and pyrophyllite all are important in natural resource exploration and characterization. Previous research has proven the ability of hyperspectral systems to uniquely identify and map these and other minerals, even in subpixel abundances [2]–[5]. Most of these capabilities can theoretically be extended to satellite altitudes. The launch of the National Aeronautics and Space Administration (NASA) Earth Observing 1 (EO-1) platform in November 2000 marks the first operational test of NASA's "New Millennium" technology, designed to test a set of advanced technology in space for land imaging. Selected Analytical Imaging and Geophysics LLC (AIG)/Commonwealth Scientific and Industrial Research Organisation (CSIRO) Hyperion analysis results demonstrating mineral mapping have previously been presented and published [6], but new details and accuracy assessment compared to airborne hyperspectral data are described here. Two case histories are presented, a "winter" Hyperion dataset (Cuprite, NV), and a "summer" Hyperion dataset (northern Death Valley, California and Nevada). Selected SNR calculations/results for other sites around the world are also summarized.

II. Comparison of Hyperion and Aircraft Hyperspectral Specifications

Imaging Spectrometers, or "Hyperspectral" sensors provide a unique combination of both spatially contiguous spectra and spectrally contiguous images of the earth's surface unavailable from other sources [2]. Research-grade airborne hyperspectral data have been available for over 20 years [4]. Current airborne sensors provide high spatial resolution (2–20 m), high-spectral resolution (10–20 nm), and high SNR ($>500:1$) data for a variety of scientific disciplines.

The Airborne Visible/Infrared Imaging Spectrometer (AVIRIS) represents the current state of the art. AVIRIS, flown by NASA/Jet Propulsion Laboratory (JPL) is a 224-channel imaging spectrometer with approximately 10-nm spectral resolution covering the 0.4–2.5-μm spectral range [7]. The sensor is

TABLE I
AVIRIS/HYPERION SENSOR CHARACTERISTICS COMPARISON

HSI Sensor	Spectral Bands	Spectral Resolution	Spatial Resolution	Swath Width	SWIR SNR
AVIRIS-High Altitude	224	10 nm	20 m	12 km	~500:1
Hyperion	242	10 nm	30 m	7.5 km	~50:1

a whiskbroom system utilizing scanning foreoptics to acquire cross-track data. The IFOV is 1 mrad. Four off-axis double-pass Schmidt spectrometers receive incoming illumination from the foreoptics using optical fibers. Four linear arrays, one for each spectrometer, provide high sensitivity in the 0.4–0.7-, 0.7–1.2-, 1.2–1.8-, and 1.8–2.5-μm regions, respectively. AVIRIS is flown as a research instrument on the NASA ER-2 aircraft at an altitude of approximately 20 km, resulting in approximately 20-m pixels and a 10.5-km swath width. Since 1998, it has also been flown on a Twin Otter aircraft at low altitude, yielding 2–4-m spatial resolution.

The launch of NASA's EO-1 Hyperion sensor in November 2000 marked the establishment of spaceborne hyperspectral mineral-mapping capabilities. Hyperion is a satellite hyperspectral sensor covering the 0.4–2.5-μm spectral range with 242 spectral bands at approximately 10-nm spectral resolution and 30-m spatial resolution from a 705-km orbit [8]. Hyperion is a pushbroom instrument, capturing 256 spectra each with 242 spectral bands over a 7.5-km-wide swath perpendicular to the satellite motion. The system has two grating spectrometers: one visible/near-infrared (VNIR) spectrometer (approximately 0.4–1.0 μm) and one SWIR spectrometer (approximately 0.9–2.5 μm). Data are calibrated to radiance using both premission and on-orbit measurements. Key AVIRIS and Hyperion characteristics are compared in Table I and discussed further in [9].

III. SITE LOCATIONS AND DESCRIPTIONS

Cuprite, NV, located approximately 200 km northwest of Las Vegas, NV (Fig. 1) is a relatively undisturbed acid-sulfate hydrothermal system in volcanic rocks exhibiting well-exposed alteration mineralogy consisting principally of kaolinite, alunite, and hydrothermal silica. The geology and alteration were previously mapped in detail [10]. Swayze [11] includes a good geologic summary, a generalized geologic map, and detailed mineral maps derived from 1990 and 1994 AVIRIS data. Cuprite has been used as a geologic remote sensing test site since the early 1980s, and many studies have been published [2], [6], [11]–[17]. The second site, in northern Death Valley, California and Nevada, is approximately 30 km southwest of Cuprite at the extreme northern end of Death Valley National Park. The geology consists principally of a Jurassic-age intrusion exhibiting quart–sericite–pyrite hydrothermal alteration [18], [19]. This site has been used as a test area for imaging spectrometers since 1983 [4], [19], [20].

This study compares mineral-mapping results of AVIRIS data acquired June 19, 1997 (f970 619t01p02_r02) to

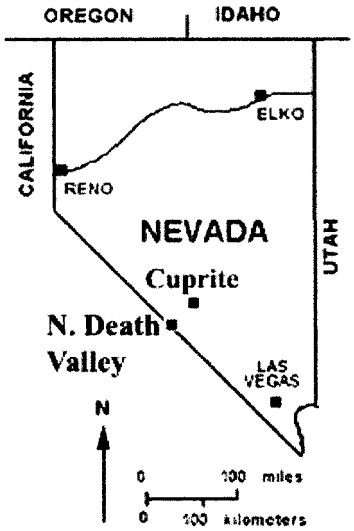

Fig. 1. Location map for the Cuprite and northern Death Valley sites.

Hyperion data collected March 1, 2001 (a winter collection, EO12 001 060_3FCD3FCC_r1_PF1_01.L1) for the Cuprite site. AVIRIS data collected June 9, 2000 (f000 609t01p03_r04) are also compared to Hyperion data collected July 23, 2001 (a summer collection, EO12 001 204_20AD20AC_r1_PF1_01.L1_A) for the northern Death Valley site. Figs. 2 and 3 show reference image subsets for the AVIRIS and Hyperion data.

IV. SNR COMPARISONS

The quality of digital remote sensing data is directly related to the level of system noise relative to signal strength. This is usually expressed as SNR, a dimensionless number that describes overall system radiometric performance [21]. System noise is tied to sensor design and takes into account factors such as detector performance/sensitivity, spatial/spectral resolution, and noise characteristics of the system electronics. Though the noise levels for a given sensor are generally fixed, for remote sensing data acquisition, the signal portion of the SNR is affected by other external factors such as solar zenith angle, atmospheric attenuation and scattering, and surface reflectance, which modify the signal available to the sensor [22].

One common means for determining an approximate SNR for remote sensing data is to use a mean/standard deviation method [7], [9]. This approach requires definition of a spectrally homogeneous area, calculation of the average spectrum for that area, and determination of the spectrally distributed standard deviation for the average spectrum. SNR are normalized to 50% reflectance for comparison. SNR calculated using this method are representative of those that can be extracted directly from the data; however, SNR for bright targets may be underestimated because of homogeneity issues at higher SNR (increasing SNR may result in breakdown of apparently homogeneous areas into multiple materials, and new homogeneous areas must be selected). Slightly higher SNR values could probably be obtained through direct analysis of the data dark current signal [7], an "Instrument SNR"; however, this is not always possible. SNR

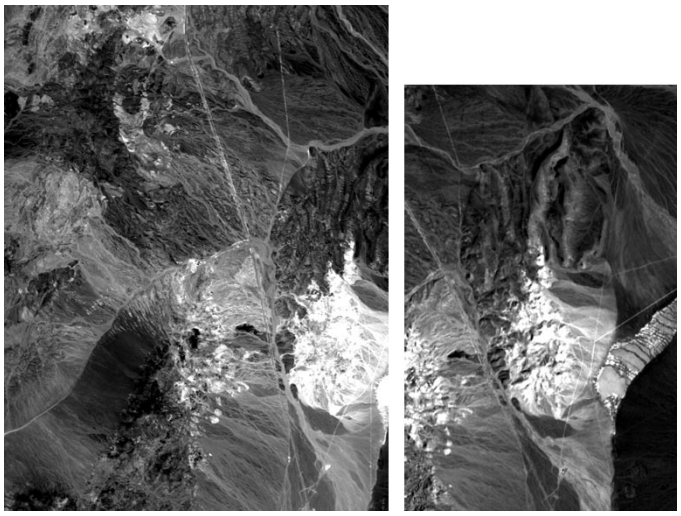

Fig. 2. Reference images (0.66 μm) showing (left) the AVIRIS and (right) Hyperion coverage of the Cuprite, NV site. The site is typically described as consisting of two hydrothermal centers [11]. These can be seen in the images as bright areas to the right and left of the road running from northwest to southeast across the scenes.

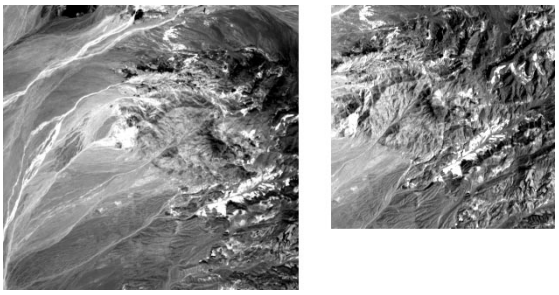

Fig. 3. Reference images (0.66 μm) showing (left) the AVIRIS and (right) Hyperion coverage of the northern Death Valley, California and Nevada site. The circular area near the center of the images is the Jurassic-age intrusion.

calculated using the mean/standard deviation method, an "Environmental SNR," is sensitive to acquisition conditions as mentioned above and, thus, should be considered a lower limit on performance.

Analysis of approximately 14 Hyperion scenes from around the world using the mean/standard deviation SNR method shows that there is a strong relationship between the acquisition time of year and the SNR of the Hyperion data [6]. Calculated SNR for Hyperion SWIR data are higher in the summer and lowest in the winter (Fig. 4).

This has a direct effect on spectral mineral mapping, with lower SWIR SNR resulting in extraction of less detail (also see AVIRIS versus Hyperion minimum noise fraction (MNF) comparison in Section V). Fig. 5 shows the SNR for the Cuprite AVIRIS (June 1997) and Hyperion (March 2001) data, as well as the calculated SNR for Hyperion data collected during July 2001 (Northern Hemisphere summer) for the northern Death Valley site. Note that this SWIR SNR is significantly higher than the calculated Cuprite SWIR SNR for the March 2001 data (SWIR SNR $\sim 60:1$ versus $25:1$).

V. Mineral Mapping

A. Methods

AIG has developed methods for analysis of hyperspectral data that allow reproducible results with minimal subjective analysis (Fig. 6) [23]. These approaches are implemented and documented within the "Environment for Visualizing Images" (ENVI) software system originally developed by AIG scientists (now an Eastman Kodak/Research Systems Inc. (RSI) commercial-off-the-shelf (COTS) product) [24]. The hyperspectral analysis methodology includes the following:

1) data preprocessing (as required);
2) correction of data to apparent reflectance using the atmospheric correction software;
3) linear transformation of the reflectance data to minimize noise and determine data dimensionality;
4) location of the most spectrally pure pixels;
5) extraction and automated identification of endmember spectra;
6) spatial mapping and abundance estimates for specific image endmembers.

A key point of this methodology is the reduction of data in both the spectral and spatial dimensions to locate, characterize, and identify a few key spectra (endmembers) that can be used to explain the rest of the hyperspectral dataset. Once these endmembers are selected, then their location and abundances can be mapped from the linearly transformed or original data. These methods derive the maximum information from the hyperspectral data themselves, minimizing the reliance on *a priori* or outside information.

1) Destriping for Hyperion Area Array Data: If required, preprocessing/data cleanup may be applied to the data prior to atmospheric correction. In the case of Hyperion data, though radiometric corrections were applied prior to data delivery to AIG, there was still a pronounced vertical striping pattern in the data (visible in individual bands, but more pronounced when using the linearly transformed data). Such striping is often seen in data acquired using pushbroom (area array) technology (e.g., Airborne Imaging Spectrometer (AIS), Hyperion) and may be caused by factors such as detector nonlinearities, movement of the slit with respect to the focal plane, and temperature effects. Previous destriping efforts suggest that a simple dark current (DC) imbalance (DC bias) of the detectors across the pixel direction of the detector array may explain the striping, and a simple per-column DC offset is sufficient to correct the problem [25].

Destriping of the Hyperion data was accomplished using custom software (following the model of software written for the original pushbroom imaging spectrometer (AIS) [19]. This approach adjusts each image column brightness (in all bands) based on a calculated offset relative to the scene average detector response. Assumptions made were that individual detectors were reasonably well behaved (stable) and that over the course of a data collect ("flightline"), that each of the cross-track detectors has covered, on the average, very similar surface materials (this second assumption is usually valid in desert environments, but may not be for other, more complex scenes). Implementation consisted of calculation of

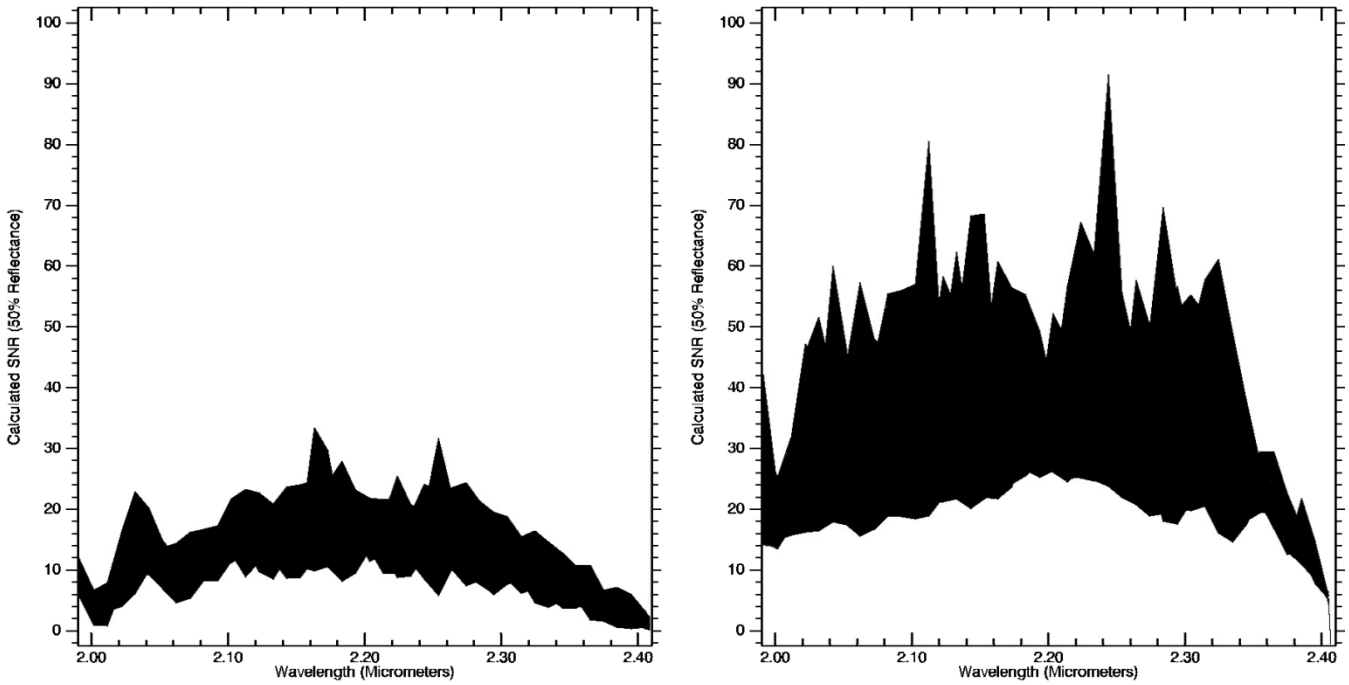

Fig. 4. Comparison of Hyperion calculated SNR for (left) "winter" data and (right) "summer" data. Filled areas indicate range of SNR for 14 Hyperion scenes.

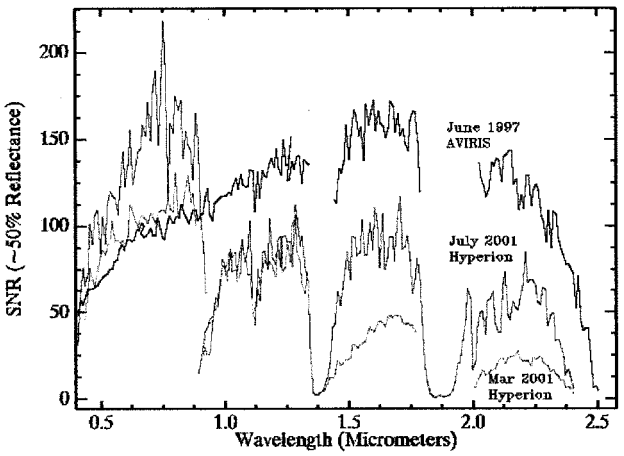

Fig. 5. SNR Comparisons for June 1997 AVIRIS, July 2001 Hyperion, and March 2001 Hyperion.

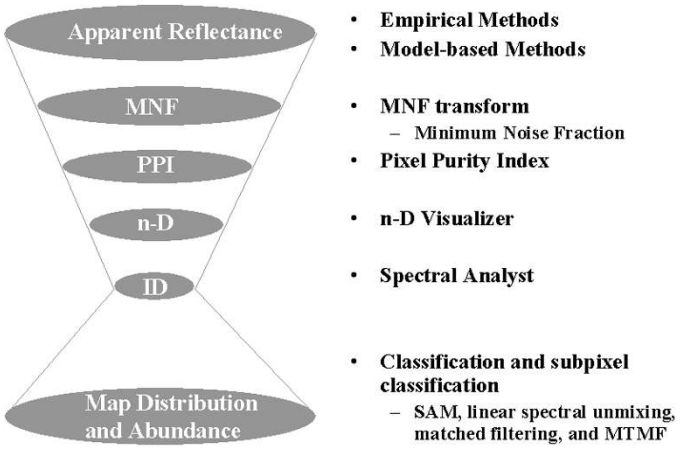

Fig. 6. AIG processing methods for hyperspectral data analysis.

an average spectrum (242 bands) for each of the 256 Hyperion detectors followed by determination of a global scene average spectrum. Each column spectrum was then subtracted from the global spectrum to determine offsets to be added to each pixel in the corresponding column. Each pixel in each column of the radiance data was then adjusted accordingly using the calculated offset. Destriping is only required for correcting the pushbroom Hyperion data, and thus no destriping was applied to the AVIRIS data.

2) Atmospheric Correction: Our analysis methods are generally applicable to both airborne and satellite data; however, the methodology requires processing radiance-calibrated data to apparent reflectance. Atmospheric CORrection Now (ACORN) [26], currently used for correction of both airborne and satellite hyperspectral data, is commercially available enhanced atmospheric model-based software that uses licensed MODTRAN4 technology to produce high-quality surface reflectance without ground measurements. The AVIRIS and Hyperion data were both converted to apparent reflectance using ACORN. Appropriate model parameters for each instrument (e.g., sensor altitude), collection date (e.g., date, time, seasonal atmospheric model), and location (e.g., latitude/longitude, average elevation) were used; otherwise, all other parameters were identical for both datasets.

3) AIG-Developed Hyperspectral Analysis: AIG-developed hyperspectral analysis methods used for both the airborne sensors and Hyperion data (implemented in the ENVI image analysis software) include spectral polishing [27], spectral data reduction using the MNF transformation [28], [29], spatial data reduction using the Pixel Purity Index (PPI) [29], an n-Dimensional Visualizer to determine image endmembers [29], identification of endmembers using their reflectance spectra [20] in the Spectral Analyst, and mineral mapping using both the Spectral

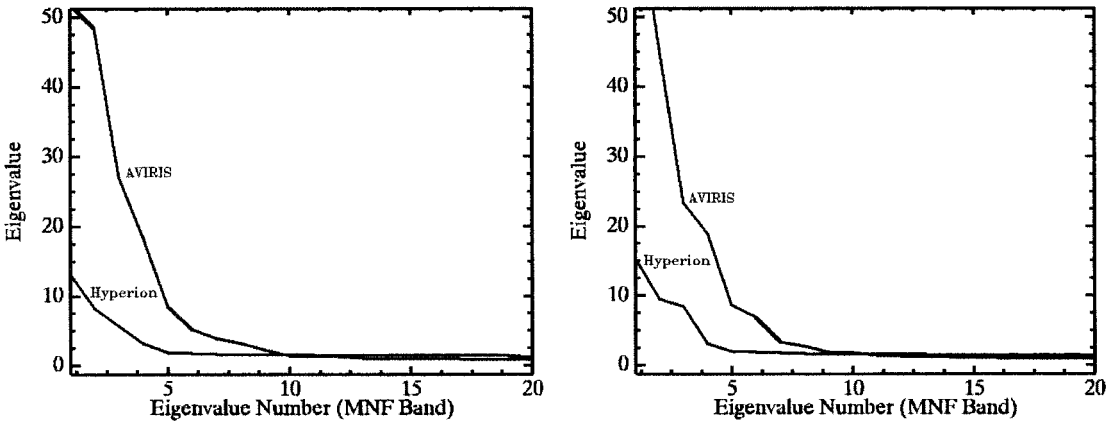

Fig. 7. MNF Eigenvalue plots for (left) the Cuprite, NV and (right) northern Death Valley, California and Nevada. AVIRIS and Hyperion data.

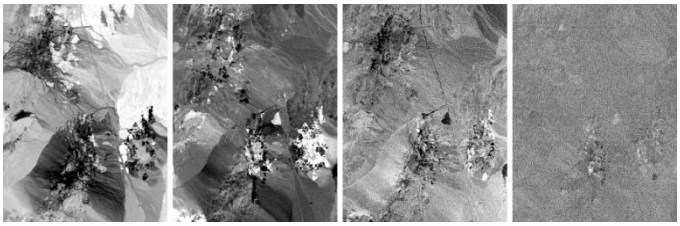

Fig. 8. MNF images for the Cuprite AVIRIS SWIR data. (Left to right) MNF band 1, MNF band 5, MNF band 10, MNF band 20.

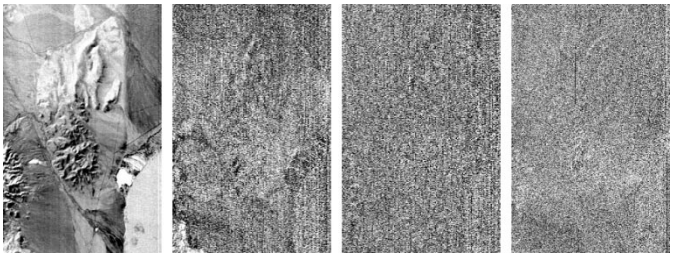

Fig. 9. MNF images for the Cuprite Hyperion SWIR data. (Left to right) MNF band 1, MNF band 5, MNF band 10, MNF band 20.

Angle Mapper (SAM) [30], and Mixture-Tuned Matched Filtering (MTMF) [31]. This approach is shown in Fig. 6 and also outlined in [23] and [29].

4) Geometric Corrections: The final step in the analysis is usually to present the results on a map base. In this case, to facilitate comparison of the Hyperion data to AVIRIS mineral-mapping results and minimize resampling artifacts, the AVIRIS data were used as the base rather than a map. The Hyperion data were geometrically corrected to match the AVIRIS data by picking ground control points (GCPs) and using a first-degree polynomial warp with nearest neighbor resampling. Approximately 20 GCPs were used, and the residual errors were on the order of two pixels. Hyperion image maps (not the full data cube!) were geocorrected to match the AVIRIS data.

B. Mapping Results

Operationally, spectral bands covering the shortwave infrared spectral range (2.0–2.4 μm) were selected, and these bands were linearly transformed using the MNF transformation. Fig. 7 shows plots of the MNF eigenvalues for the two datasets.

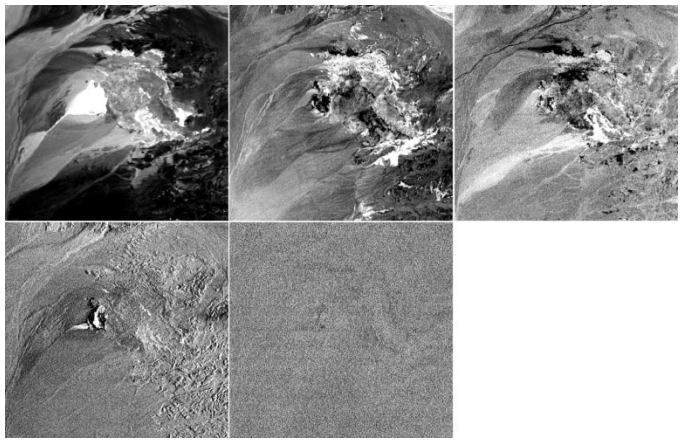

Fig. 10. MNF images for the northern Death Valley AVIRIS SWIR data. (Left to right) MNF band 1, MNF band 5, MNF band 8, MNF band 10, MNF band 20.

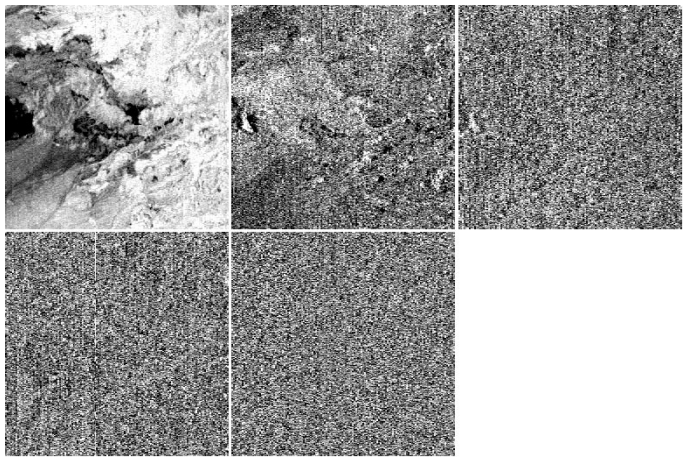

Fig. 11. MNF images for the northern Death Valley Hyperion SWIR data. (Left to right) MNF band 1, MNF band 5, MNF band 8, MNF band 10, MNF band 20.

Higher eigenvalues generally indicate higher information content. The MNF results indicate that, for both cases, the AVIRIS data contain significantly more information than the Hyperion data covering approximately the same spatial area and spectral range. The actual data dimensionality is usually determined by comparing both the eigenvalue plots and the

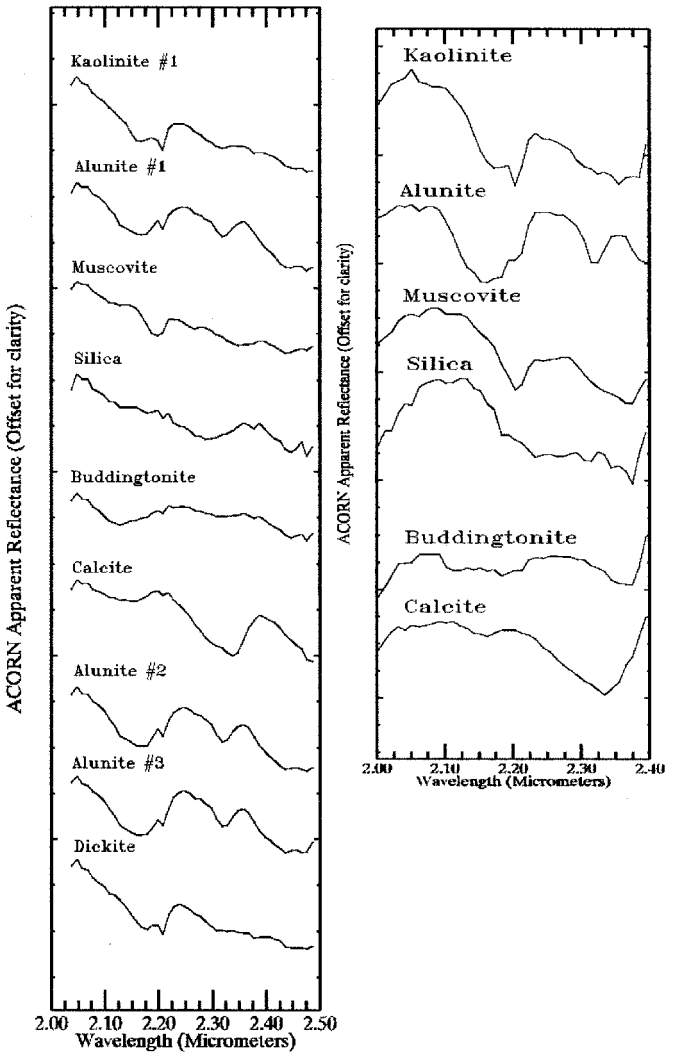

Fig. 12. Comparison of selected (left) AVIRIS endmember spectra and (right) Hyperion endmember spectra for the Cuprite, NV site. Note that AVIRIS detected several varieties of alunite plus an additional kaolinite-group mineral (dickite) that were not detectable using the Hyperion data.

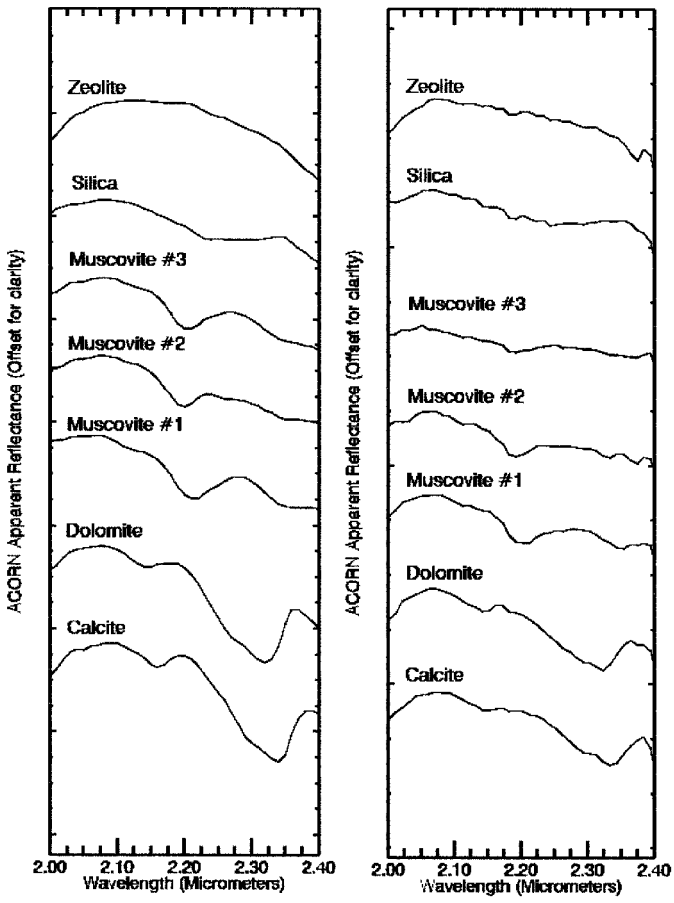

Fig. 13. Comparison of selected (left) AVIRIS endmember (mean) spectra and (right) Hyperion endmember (mean) spectra for the northern Death Valley, California and Nevada site.

MNF images for each dataset (Figs. 7–11). In the case of the Cuprite AVIRIS, the MNF analysis indicates a dimensionality of approximately 20. The Cuprite Hyperion data exhibits dimensionality of approximately six. For the northern Death Valley site, AVIRIS shows dimensionality of approximately 20 and Hyperion approximately eight.

The top MNF bands for each dataset (corresponding to the approximate dimensionality), which contain most of the spectral information [28], were used to determine the most likely endmembers using the PPI procedure. These potential endmember spectra were then loaded into an n-dimensional (n-D) scatterplot and rotated in real time on the computer screen until "points" or extremities on the scatterplot were exposed [29]. These projections were "painted" using region-of-interest (ROI) definition procedures and then rotated again in three or more dimensions (three or more MNF bands) to determine if their signatures were unique in the MNF data. While this portion of the analysis presents the greatest opportunity for subjective bias, iterative n-D rotation and examination of remaining data dimensionality after selection of each subsequent endmember minimizes this effect and maximizes the chance of reproducible results. Additionally, "class collapsing," which rotates selected endmembers to a common projection and enhances remaining endmember locations in the scatterplots, allows an analyst to determine when all of the inherent endmembers have been located.

Once a set of unique pixels was defined using the n-D analysis technique, then each separate projection on the scatterplot (corresponding to a pure endmember) was exported to a ROI in the image. Mean spectra were then extracted for each ROI from the apparent reflectance data to act as endmembers for spectral mapping for both the Cuprite Site (Fig. 12) and the northern Death Valley site (Fig. 13). These endmembers or a subset of these endmembers (in the case of AVIRIS) were used for subsequent classification and other processing. MTMF [31], a spectral matching method, was used to produce image maps showing the distribution and abundance of selected minerals (note: MNF endmember spectra, not reflectance spectra, are used in the MTMF). The results are generally presented either as grayscale images with values from 0.0 to 1.0 (not shown), which provide a means of estimating mineral abundance, or as color mineral maps showing the spectrally predominant material for each pixel (Figs. 14–16). Basic mineral mapping was performed for the Cuprite site (Fig. 14). Two image maps were

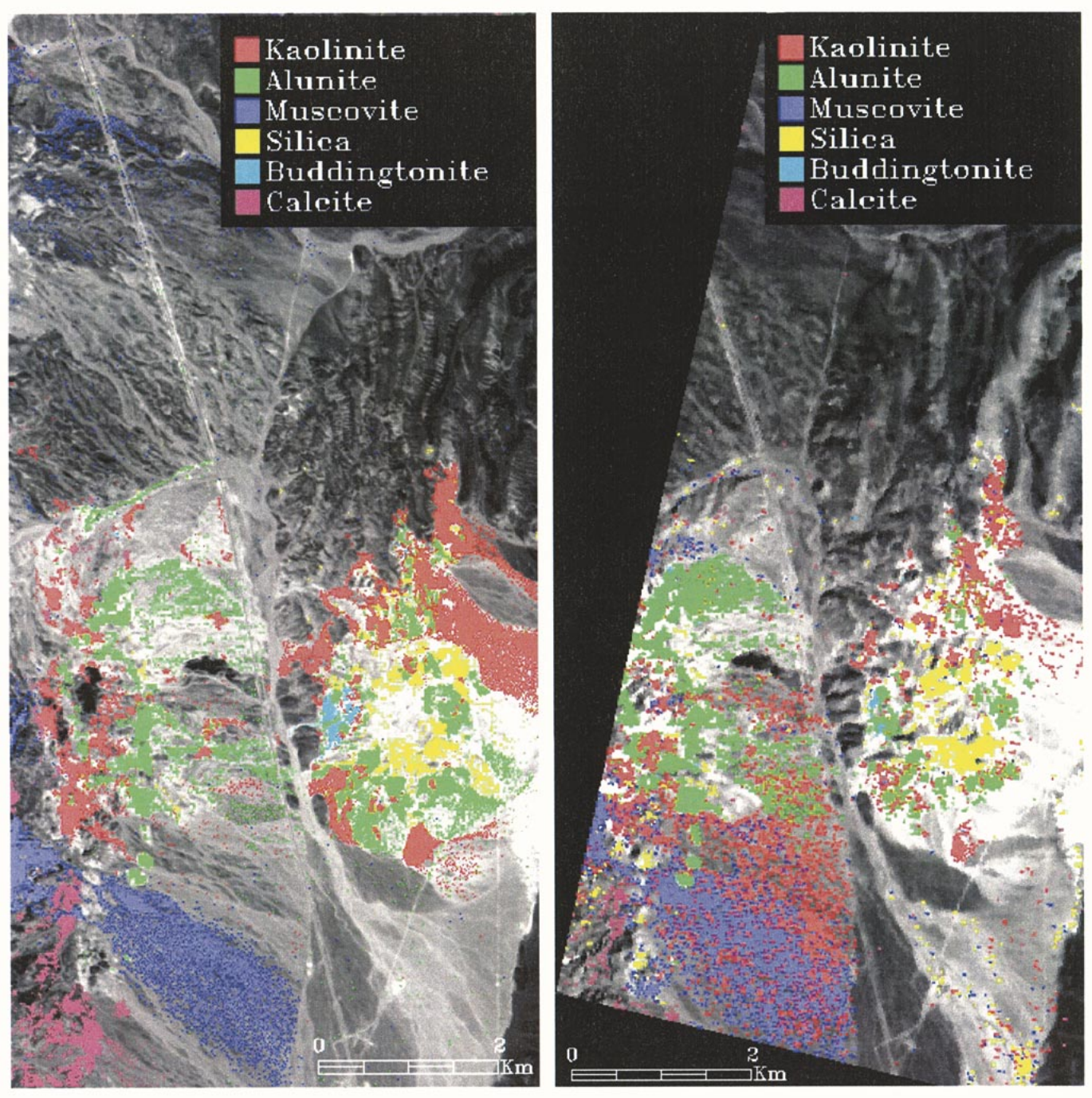

Fig. 14. MTMF mineral maps for (left) AVIRIS and (right) Hyperion produced for the endmembers in Fig. 12 for the Cuprite, NV site. Colored pixels show the spectrally predominant mineral at concentrations greater than 10%.

produced for the northern Death Valley site: 1) a detailed mineral map showing minerals and mineral variability (Fig. 15) and 2) a basic mineral map produced by combining occurrences of similar minerals (Fig. 16).

C. Discussion

Visual comparison of the AVIRIS and Hyperion mineral maps for both sites shows that Hyperion generally identifies similar minerals and produces similar mineral-mapping results to AVIRIS. Our results indicate, however, that the lower SNR of the Hyperion data does affect the ability to extract characteristic spectra and identify individual minerals (Figs. 12–15). Specifically, compare the Hyperion buddingtonite spectrum in Fig. 12, which does not clearly show the characteristic buddingtonite spectral feature shape near 2.11 μm, to the well-resolved feature extracted from AVIRIS (Fig. 12) and other hyperspectral aircraft data [11], [14]. Note that while it generally appears that the difference in pixel size (30 m for Hyperion versus approximately 16 m for AVIRIS) is minimal (causing only slight loss of spatial detail in Hyperion results), some of the spectral difference could be an effect of the

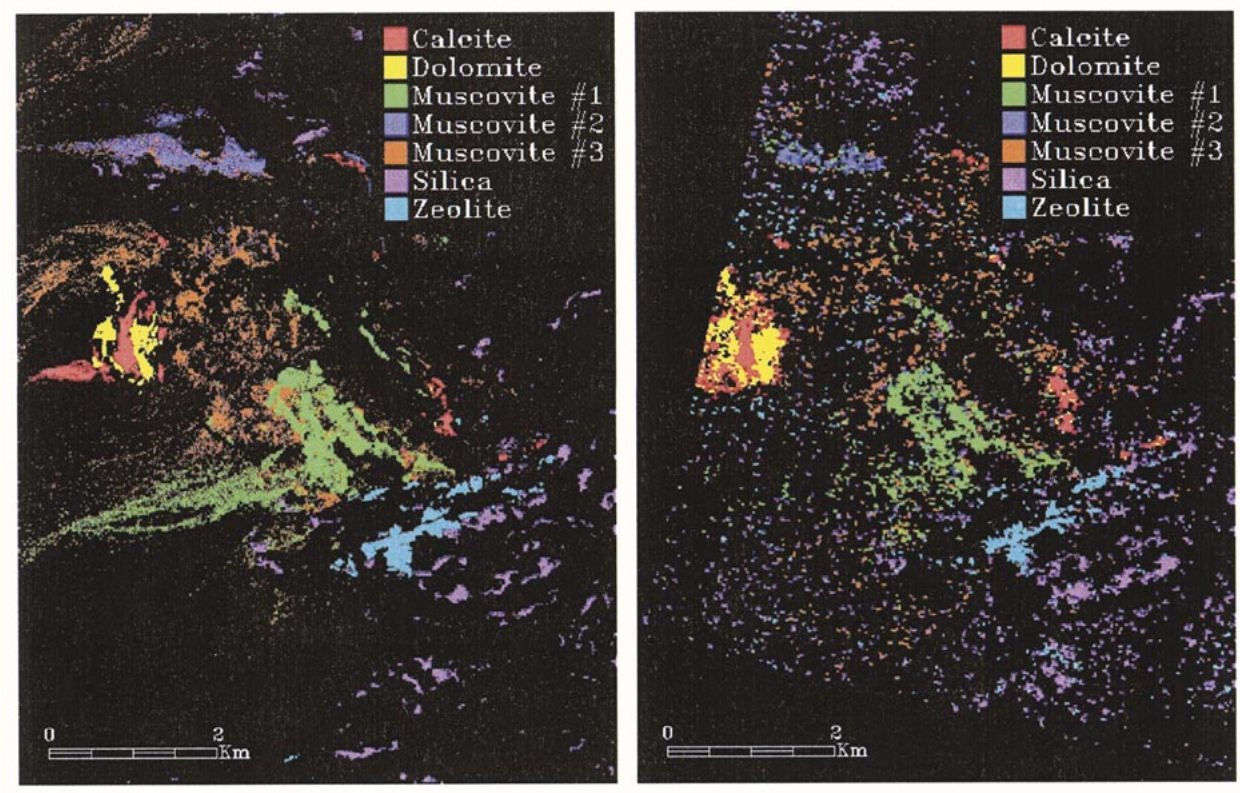

Fig. 15. MTMF mineral maps for (left) AVIRIS and (right) Hyperion produced for the endmembers in Fig. 13 for the northern Death Valley, California and Nevada site. Colored pixels show the spectrally predominant mineral at concentrations greater than 10%.

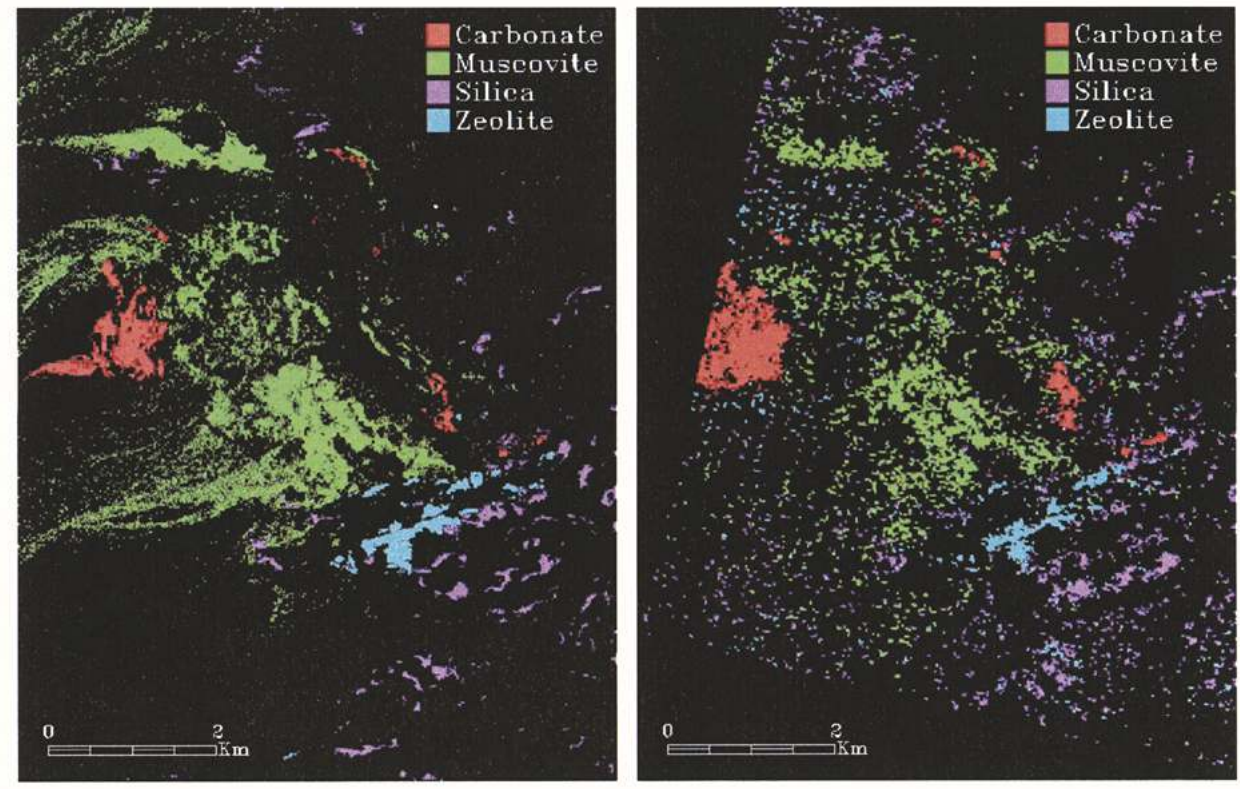

Fig. 16. MTMF mineral maps for (left) AVIRIS and (right) Hyperion produced for a subset of the endmembers in Fig. 13 for the northern Death Valley, California and Nevada site. Colored pixels show the spectrally predominant mineral group at concentrations greater than 10%.

TABLE II
CONFUSION MATRIX COMPARING CUPRITE HYPERION MTMF MINERAL-MAPPING RESULTS TO AVIRIS "GROUND TRUTH" MTMF BASIC MINERAL-MAPPING RESULTS (EXCLUDES UNCLASSIFIED PIXELS). OVERALL ACCURACY IS 75%. KAPPA COEFFICIENT IS 0.67

	AVIRIS Ground Truth (Percent)						
Hyperion Class	Kaolinite %	Alunite %	Muscovite %	Silica%	Buddingtonite%	Calcite %	Total
Kaolinite	**74.48**	16.64	25.32	10.68	5.33	3.54	36.44
Alunite	14.28	**79.86**	0.06	5.39	59.17	0.00	31.47
Muscovite	7.12	0.70	**72.77**	2.15	0.00	9.45	20.76
Silica	3.72	2.14	1.00	**80.16**	0.00	6.69	8.73
Buddingtonite	0.02	0.34	0.00	0.00	**35.50**	0.00	0.55
Calcite	0.39	0.32	0.85	1.62	0.00	**80.31**	2.05
Total	100.00	100.00	100.00	100.00	100.00	100.00	100.00

pixel size, causing greater mixing in the Hyperion data for relatively small buddingtonite occurrences. Other examples of the limitations of Hyperion imposed by lower SNR than AVIRIS include the inability to separate mineral variability such as that caused by cation substitution (K versus Na in alunites, and Al versus Fe substitution in micas) and crystal structure differences (kaolinite versus dickite) at SNR less than approximately 50 : 1 (Figs. 12 and 14). Our analysis indicates that the Cuprite Hyperion data do not allow extraction of the same level of detailed mineralogic information as AVIRIS [6], [11]. Fig. 14 shows only a basic AVIRIS mineral map. Other researchers have demonstrated mapping of other minerals using AVIRIS at the Cuprite site that were not detected using the March 2001 Hyperion data [11]. Finally, determination of abundances for minerals identified by AVIRIS and Hyperion is possible [4]–[6], [29], but not illustrated here. Actually, Hyperion performs quite well considering the overall SWIR SNR.

VI. ACCURACY ASSESSMENT AND ERROR ANALYSIS

A. General

While visual comparison of the Hyperion and AVIRIS MTMF image maps for Cuprite (Fig. 14) and northern Death Valley (Fig. 15) using the AVIRIS data as the "ground truth" indicates that, in general, using these mapping methods, the AVIRIS and Hyperion produce similar mapping results, detailed direct comparison of the mapping results using a confusion matrix approach [32] demonstrates that the correspondence is not as great as may be thought from visual comparison. Comparison of the AVIRIS and Hyperion MTMF spectral mapping results for the both sites shows that many pixels classified using AVIRIS are unclassified on Hyperion (up to 60%, but variable by mineral). These are errors of omission and are probably explained by the differences in SNR between the two datasets. Some spectral features are simply below the level of detection on the Hyperion data.

B. Cuprite Accuracy Assessment

Confusion matrix analysis for the Cuprite site, excluding the unclassified areas, illustrates that accurate mapping is possible when Hyperion is able to identify a specific mineral. (The three alunite classes and the kaolinite–dickite classes shown for AVIRIS in Fig. 14 were combined for the purposes of this evaluation.) Using the AVIRIS combined mineral map yields an approximately 76% overall agreement of Hyperion to AVIRIS for the Cuprite site, with a Kappa Coefficient of 0.67 (Table II). This highlights errors of commission (where pixels mapped as one mineral by AVIRIS are mapped as another mineral by Hyperion). First, some pixels unclassified using AVIRIS are misclassified as a specific mineral on Hyperion (around 10% commission error). Additionally, some pixels classified by AVIRIS as specific minerals are misclassified as different minerals on Hyperion ($\sim$ 25% commission error). Specifically, there is minor classification error between the following: kaolinite mapped by Hyperion as muscovite (7%), kaolinite as silica (4%), alunite as silica (2%), muscovite as silica (1%), muscovite as calcite (1%), silica as muscovite (2%), silica as calcite (2%), silica as alunite (5%), buddingtonite as kaolinite (5%), calcite as kaolinite (4%), calcite as silica (7%), and calcite as muscovite (9%). Moderate errors occur between the following: kaolinite mapped by Hyperion as alunite (14%), alunite as kaolinite (17%), and silica as kaolinite (11%). The highest errors occur between the following: muscovite mapped by Hyperion as kaolinite (25%) and buddingtonite mapped by Hyperion as alunite (59%). The general relationship between mineralogy and mapping errors indicates that the highest errors occur for minerals with more similar spectral signatures (Fig. 12 and Table II). Table II summarizes the relationships between minerals.

C. Northern Death Valley Accuracy Assessment

Confusion matrix analysis for the northern Death Valley site, including the unclassified areas, again shows that Hyperion has difficulty locating many areas with weak mineral signatures

TABLE III
CONFUSION MATRIX COMPARING HYPERION NORTHERN DEATH VALLEY MTMF MINERAL-MAPPING RESULTS TO AVIRIS "GROUND TRUTH" MTMF DETAILED MINERAL-MAPPING RESULTS (INCLUDES UNCLASSIFIED PIXELS). OVERALL ACCURACY IS 86%. KAPPA COEFFICIENT IS 0.25

	AVIRIS Ground Truth (Percent)								
Hyperion Class	Unclassified	Calcite	Dolomite	Muscovite #1	Muscovite #2	Muscovite #3	Silica	Zeolite	Total
Unclassified	**89.23**	24.51	21.42	59.58	52.71	77.26	65.50	48.42	85.97
Calcite	0.82	**62.40**	13.16	0.00	0.15	0.25	0.16	0.11	1.25
Dolomite	0.52	11.87	**65.23**	0.00	0.00	0.00	0.03	0.05	0.90
Muscovite #1	0.73	0.08	0.00	**34.61**	7.11	9.35	0.47	0.00	2.14
Muscovite #2	0.19	0.00	0.00	0.85	**36.14**	2.61	0.03	0.00	0.56
Muscovite #3	2.89	0.08	0.00	3.37	2.13	**8.11**	0.85	0.37	3.01
Silica	4.27	0.15	0.19	1.54	1.76	1.45	**30.94**	3.10	4.44
Zeolite	1.34	0.91	0.00	0.05	0.00	0.97	2.01	**47.94**	1.74
Total	100.00	100.00	100.00	100.00	100.00	100.00	100.00	100.00	100.00

TABLE IV
CONFUSION MATRIX COMPARING HYPERION NORTHERN DEATH VALLEY MTMF MINERAL-MAPPING RESULTS TO AVIRIS "GROUND TRUTH" MTMF DETAILED MINERAL-MAPPING RESULTS. EXCLUDES UNCLASSIFIED PIXELS. OVERALL ACCURACY IS 76%. KAPPA COEFFICIENT IS 0.71

	AVIRIS Ground Truth (Percent)							
Hyperion Class	Calcite	Dolomite	Muscovite #1	Muscovite #2	Muscovite #3	Silica	Zeolite	Total
Calcite	**82.66**	16.75	0.00	0.31	1.11	0.46	0.21	11.46
Dolomite	15.73	**83.01**	0.00	0.00	0.00	0.09	0.10	9.74
Muscovite #1	0.10	0.00	**85.62**	15.04	41.13	1.37	0.00	33.07
Muscovite #2	0.00	0.00	2.11	**76.43**	11.49	0.09	0.00	8.62
Muscovite #3	0.10	0.00	8.33	4.50	**35.65**	2.46	0.72	10.14
Silica	0.20	0.24	3.81	3.72	6.36	**89.70**	6.00	14.76
Zeolite	1.21	0.00	0.13	0.00	4.26	5.83	**92.96**	12.21
Total	100.00	100.00	100.00	100.00	100.00	100.00	100.00	100.00

(Table III). Excluding the unclassified areas provides an assessment of how well Hyperion performs when specific minerals are identified for individual pixels and illustrates that improved mapping (compared to the lower SNR Cuprite Hyperion data) is possible with higher SNR (Table IV). The SNR for the northern Death Valley Hyperion data is approximately 60 : 1 or about twice that of the Cuprite Hyperion data (Fig. 5). The implications of the decreased Hyperion winter SNR are evident in endmember spectra extracted from both the Cuprite AVIRIS and Hyperion (Fig. 12) and the northern Death Valley Hyperion data (Fig. 13). While the Cuprite Hyperion data allow basic mineral identification (no separation of within-species variability), more details (additional endmembers) are detected and mapped using the higher SNR AVIRIS and Hyperion data. This is also important for geologic/mineral mapping, because higher SNR allows separation of similar endmembers such as calcite from dolomite (Figs. 13 and 15) and within-species variability such as kaolinite versus dickite (Fig. 12). In the northern Death Valley case, the relatively high Hyperion SNR allows detection of three different mica endmembers with different aluminum substitution [4]. Previous investigations have indicated that SNR is critical for this determination [4], [6].

Visual comparison of the detailed mapping results for the northern Death Valley site shows generally good correspon-

TABLE V
CONFUSION MATRIX COMPARING HYPERION NORTHERN DEATH VALLEY MTMF MAPPING RESULTS TO AVIRIS "GROUND TRUTH" MTMF BASIC (COMBINED MINERALS) MAPPING RESULTS. EXCLUDES UNCLASSIFIED PIXELS. OVERALL ACCURACY IS 94%. KAPPA COEFFICIENT IS 0.91

	AVIRIS Ground Truth (Percent)				
Hyperion Class	Carbonate	Muscovite	Silica	Zeolite	Total
Carbonate	**99.01**	0.44	0.55	0.31	21.19
Muscovite	0.11	**93.23**	3.92	0.72	51.83
Silica	0.22	4.72	**89.70**	6.00	14.76
Zeolite	0.66	1.61	5.83	**92.96**	12.21
Total	100.00	100.00	100.00	100.00	100.00

dence between the AVIRIS and Hyperion mapping. Confusion matrix results excluding the unclassified pixels show overall accuracy of approximately 76% for the Hyperion mapping as compared to AVIRIS, with a Kappa coefficient of 0.71. Table IV does indicate that, again, there is considerable difficulty separating similar mineralogy, in this case, the three muscovite varieties. At the calculated 60 : 1 SNR, these identifications appear to be near the detection limit. Grouping similar minerals together (calcite with dolomite, and combining the three muscovites) results in dramatic identification and mapping improvements (Fig. 16, Table V) and a more direct comparison to the Cuprite results (Table II). Overall accuracy is boosted to greater than 94% and the Kappa coefficient to 0.91 (Fig. 16, Table V).

D. Factors Affecting Accuracy Assessment

While these comparisons serve to highlight the accuracy and overall performance of the Hyperion data compared to AVIRIS for these sites, several other issues may affect the accuracy assessment. These include the following:

1) data coverage (spatial extent) of the two datasets: they cover substantially the same ground, but not exactly (affects unclassified class—masking was used to exclude areas that did not overlap);
2) data pixel size (AVIRIS is $\sim$ 16 m, Hyperion 30 m);
3) image acquisition differences (date/time, atmospheric conditions, actual SNR);
4) slightly different spectral characteristics (varying band centers and spectral resolution);
5) different image-based endmember spectra used for MTMF (endmember spectra not identical);
6) MTMF threshold consistency and class combining (AVIRIS);
7) Hyperion-to-AVIRIS image registration accuracy.

We are not able at this time to determine the relative importance of these other possible factors, other than to say that they appear to be subordinate to the larger variability problem imposed by seasonal SNR effects. Finally, while the AVIRIS data represent the best "ground truth" available and have been spot checked using field mapping and spectral measurements, they have not been and cannot be ground checked for accuracy on a pixel-by-pixel basis.

VII. CONCLUSION

Results at the Cuprite, Nevada and northern Death Valley sites establish that data from the Hyperion SWIR spectrometer (2.0–2.4 μm) can be used to produce useful geologic (mineralogic) information. Comparison of Hyperion data to airborne hyperspectral data (AVIRIS) show that Hyperion provides the ability to remotely map basic surface mineralogy. Minerals mapped at the two sites include calcite, dolomite, kaolinite, alunite, buddingtonite, muscovite (three varieties), hydrothermal silica, and zeolites. These case histories demonstrate the analysis methodologies and level of information available from these Hyperion data. They also demonstrate the viability of Hyperion as a means of extending hyperspectral mineral mapping to areas not accessable to aircraft sensors.

AVIRIS data collected during June 1997 (Cuprite) and June 2000 (northern Death Valley) served as the "ground truth" for this investigation. Comparison of Hyperion results for Cuprite (March 2001) and northern Death Valley (July 2001) to the known mineralogy derived from the AVIRIS data generally validate on-orbit mineral mapping and Hyperion performance. Standardized hyperspectral data processing methods applied to the Hyperion data lead to definition of specific key minerals; however, it is more difficult (than for AVIRIS) to extract the information because of the Hyperion data's lower SNR. The effect of this reduced response compared to AVIRIS is lower data dimensionality; thus, fewer endmembers can be identified and mapped than with AVIRIS. Accuracy assessment and error analysis indicates that with Hyperion data that, in many cases, mineral identification is not possible where specific minerals are known to exist. In addition, Hyperion often confuses similar minerals that are separable using AVIRIS.

The Hyperion data demonstrate the importance of high SNR performance for hyperspectral sensors. The Cuprite Hyperion data represent an "early" Hyperion acquisition for the Northern Hemisphere (a winter scene—low solar zenith angle); thus, the SWIR SNR is approximately 25 : 1. These data allow only basic mineral mapping, and minerals with similar spectral signatures are often confused. The northern Death Valley Hyperion scene was collected under optimum (summer—high solar zenith angle) conditions and exhibits SWIR SNR as high as approximately 60 : 1. These data allow more detailed mineral mapping, including within-species variability; however, this capability is at the detection limit of current Hyperion SNR levels. Combining minerals to form a basic mineral map results in improved mapping with greater than 94% correspondence between AVIRIS and Hyperion at the northern Death Valley site. The level of mineralogic information available from the Hyperion data is directly tied to the SNR.

As a technology demonstration, Hyperion performs satisfactorily for mineral identification and mapping. We expect (and have demonstrated) improved mineral identification and mapping results from "summer" season Hyperion acquisitions with higher SNR. These improvements principally take the form of mapping of subtle distinctions such as determining the difference between calcite and dolomite and mapping within-species

variability caused by molecular substitution (e.g., aluminum substitution in micas). Unfortunately, Hyperion data collected under less than optimum conditions (winter season, dark targets) have marginal SWIR SNR and allow mapping of only the most basic mineral occurrences and mineral differences. This results in a recommendation that future HSI satellite sensors have significantly higher SNR performance specifications than Hyperion for the SWIR (at least 100 : 1 based on dark current measurements).

ACKNOWLEDGMENT

AVIRIS data were provided by JPL. ACORN is a trademark of ImSpec Associates, LLC. ENVI is a registered trademark of Research Systems Inc., Boulder, CO. Pixel Purity Index (PPI), n-Dimensional Visualizer, Spectral Analyst, and Mixture-Tuned Matched Filter (MTMF) are all trademarks of Research Systems Inc.

REFERENCES

[1] R. N. Clark, T. V. V. King, M. Klejwa, and G. A. Swayze, "High spectral resolution spectroscopy of minerals," *J. Geophys. Res.*, vol. 95, no. B8, pp. 12 653–12 680, 1990.

[2] A. F. H. Goetz, G. Vane, J. E. Solomon, and B. N. Rock, "Imaging spectrometry for Earth remote sensing," *Science*, vol. 228, pp. 1147–1153, 1985.

[3] F. A. Kruse and A. B. Lefkoff, "Knowledge-based geologic mapping with imaging spectrometers," *Remote Sens. Rev.*, vol. 8, pp. 3–28, 1993.

[4] F. A. Kruse, J. W. Boardman, and J. F. Huntington, "Fifteen years of hyperspectral data: Northern Grapevine Mountains, Nevada," in *Proc. 8th JPL Airborne Earth Science Workshop*, vol. 99–17. Pasadena, CA, 1999, pp. 247–258.

[5] J. W. Boardman and F. A. Kruse, "Automated spectral analysis: A geologic example using AVIRIS data, North Grapevine Mountains, Nevada," in *Proce. 10th Thematic Conf. on Geologic Remote Sensing*, Ann Arbor, MI, 1994, pp. I-407–I-418.

[6] F. A. Kruse, J. W. Boardman, and J. F. Huntington, "Comparison of EO-1 hyperion and airborne hyperspectral remote sensing data for geologic applications," in *Proc. SPIE Aerospace Conf.*, Big Sky, MO, Mar. 9–16, 2002, 6.0102, p. 12.

[7] R. O. Green, B. Pavri, J. Faust, and O. Williams, "AVIRIS radiometric laboratory calibration, inflight validation, and a focused sensitivity analysis in 1998," in *Proc. 8th JPL Airborne Earth Science Workshop*, vol. 99–17. Pasadena, CA, 1999, pp. 161–175.

[8] J. Pearlman, S. Carman, P. Lee, L. Liao, and C. Segal, "Hyperion imaging spectrometer on the new millennium program Earth Orbiter-1 system," in *Proc. Int. Symp. Spectral Sensing Research (ISSSR), Systems and Sensors for the New Millennium*, 1999.

[9] R. O. Green, B. E. Pavri, and T. G. Chrien, "On-orbit radiometric and spectral calibrat ion characteristics of EO-1 Hyperion derived with an underflight of AVIRIS and *in situ* measurements at Salar de Arizaro, Argentina," *IEEE Trans. Geosci. Remote Sensing*, vol. 41, pp. 1194–1203, June 2003.

[10] R. P. Ashley and M. J. Abrams, "Alteration mapping using multispectral images—Cuprite Mining District, Esmeralda County, Nevada," U.S. Geological Survey , Reston, VA, Open File Rep. 80–367, 1980.

[11] G. A. Swayze, "The hydrothermal and structural history of the Cuprite Mining District, Southwestern Nevada: An integrated geological and geophysical approach," Ph.D. thesis, Univ. Colorado, Boulder, CO, 1997.

[12] A. F. H. Goetz and V. Strivastava, "Mineralogical mapping in the Cuprite Mining district," in *Proc. Airborne Imaging Spectrometer (AIS) Data Analysis Workshop*, vol. 85–41, 1985, pp. 22–29.

[13] H. Shipman and J. B. Adams, "Detectability of minerals on desert alluvial fans using reflectance spectra," *J. Geophys. Res.*, vol. 92, no. B10, pp. 10 391–10 402, 1987.

[14] F. A. Kruse, K. S. Kierein-Young, and J. W. Boardman, "Mineral mapping at Cuprite, Nevada with a 63 channel imaging spectrometer," *Photogramm. Eng. Remote Sens.*, vol. 56, no. 1, pp. 83–92, 1990.

[15] S. J. Hook, "The combined use of multispectral remotely sensed data from the short wave infrared (SWIR) and thermal infrared (TIR) for lithological mapping and mineral exploration," in *Proc. 5th Australasian Remote Sensing Conf.*, vol. 1, Perth, Australia, 1990, pp. 371–380.

[16] G. A. Swayze, R. L. Clark, S. Sutley, and A. J. Gallagher, "Groundtruthing AVIRIS mineral mapping at Cuprite, Nevada," in *Summaries of the 3rd Annual JPL Airborne Geosciences Workshop*, vol. 1, AVIRIS Workshop. Pasadena, CA, 1992, JPL Pub. 92–14, pp. 47–49.

[17] A. F. H. Goetz and B. Kindel, "Understanding unmixed AVIRIS images in Cuprite, NV using coincident HYDICE data," in *Proc. 6th JPL Airborne Earth Science Workshop*, vol. 1. Pasadena, CA, 1996, pp. 96–4.

[18] C. T. Wrucke, R. S. Werschkey, G. L. Raines, R. J. Blakely, D. B. Hoover, and M. S. Miller, "Mineral resources and mineral resource potential of the Little Sand Spring Wilderness study area, Inyo County, California," U.S. Geological Survey, Reston, VA, Open File Rep. 84–557, 1984.

[19] F. A. Kruse, "Use of airborne imaging spectrometer data to map minerals associated with hydrothermally altered rocks in the Northern Grapevine Mountains, Nevada and California," *Remote Sens. Environ.*, vol. 24, no. 1, pp. 31–51, 1988.

[20] F. A. Kruse, A. B. Lefkoff, and J. B. Dietz, "Expert system-based mineral mapping in Northern Death Valley, California/Nevada using the Airborne Visible/Infrared Imaging Spectrometer (AVIRIS)," *Remote Sens. Environ.*, vol. 44, pp. 309–336, May-June 1993.

[21] R. N. Collwell, Ed., *Manual of Remote Sensing*, 2nd ed: Amer. Soc. Photogrammetry and Remote Sensing, 1983, p. 1196.

[22] R. N. Collwell, Ed., *Manual of Remote Sensing*, 2nd ed: Amer. Soc. Photogrammetry and Remote Sensing, 1983, pp. 344–363.

[23] F. A. Kruse and J. W. Boardman, "Characterization and mapping of Kimberlites and related diatremes using hyperspectral remote sensing," in *Proc. 2000 IEEE AeroSpace Conf.*, Big Sky, MO, Mar. 18–24, 2000.

[24] Research Systems, Inc., *ENVI User's Guide*. Boulder, CO: Research Systems, Inc., 2001.

[25] J. D. Dykstra and D. B. Segal, "Analysis of AIS data of the recluse oil field, recluse, wyoming," in *Proc. AIS workshop*, vol. 85–41, Pasadena, CA, Apr. 8–10, 1985, pp. 86–91.

[26] AIG, *ACORN User's Guide, Stand Alone Version*. Boulder, CO: Analytical Imaging and Geophysics LLC, 2001.

[27] J. W. Boardman, "Post-ATREM polishing of AVIRIS apparent reflectance data using EFFORT: A lesson in accuracy versus precision," in *Summaries 7th JPL Airborne Earth Science Workshop*, vol. 1. Pasadena, CA, 1998.

[28] A. A. Green, M. Berman, B. Switzer, and M. D. Craig, "A transformation for ordering multispectral data in terms of image quality with implications for noise removal," *IEEE Trans. Geosci. Remote Sensing*, vol. 26, pp. 65–74, Jan. 1988.

[29] J. W. Boardman, "Automated spectral unmixing of AVIRIS data using convex geometry concepts," in *Summaries 4th JPL Airborne Geoscience Workshop*, vol. 1. Pasadena, CA, 1993, 93–26, pp. 11–14.

[30] F. A. Kruse, A. B. Lefkoff, J. B. Boardman, K. B. Heidebrecht, A. T. Shapiro, P. J. Barloon, and A. F. H. Goetz, "The spectral image processing system (SIPS)—Interactive visualization and analysis of imaging spectrometer data," *Remote Sens. Environ.*, vol. 44, pp. 145–163, May-June 1993.

[31] J. W. Boardman, "Leveraging the high dimensionality of AVIRIS data for improved sub-pixel target unmixing and rejection of false positives: Mixture tuned matched filtering," in *Summaries of the 7th Annu. JPL Airborne Geoscience Workshop*. Pasadena, CA, 1998.

[32] J. A. Richards, *Remote Sensing Digital Image Analysis, An Introduction*. New York: Springer-Verlag, 1994, pp. 271–275.

Fred A. Kruse (M'95) received the B.S degree from the University of Massachusetts, Amherst, and the M.S. and Ph. D. degrees from the Colorado School of Mines, Golden, in 1976, 1984, and 1987, respectively, all in geology.

He has been involved in multispectral, hyperspectral, and SAR remote sensing research and applications for over 20 years in positions with the U.S. Geological Survey, Golden, CO, the University of Colorado, Boulder, and in private industry. He is currently Senior Scientist with Analytical Imaging and Geophysics, LLC, Boulder, CO, and also serves as an Adjunct Assistant Professor with the Department of Geological Sciences, University of Colorado. His primary scientific interests are in the application of remote sensing technology to exploration and understanding of ore deposits and the development of knowledge-based techniques for spectral identification and mapping of geology, man-made materials, vegetation, and near-shore marine environments. He is also one of the original developers of the remote sensing analysis software package ENVI, "The Environment for Visualizing Images."

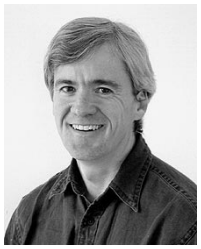

Joseph W. Boardman received the B.S. degree from the University of Oklahoma, Norman, the M.S. degree from the Colorado School of Mines, Golden, and the Ph. D. degree from the University of Colorado (UC), Boulder, in 1983, 1985, and 1991, respectively, all in geophysics.

After UC, he enjoyed a Postdoctoral research fellowship with the Commonwealth Scientific and Industrial Research Organisation, Sydney, Australia, working with J. Huntington. From 1993 to 1995, he was a Research Associate with CSES, University of Colorado, Boulder. His current research as Senior Geophysicist and Founding Partner of Analytical Imaging and Geophysics, LLC, Boulder, CO, applies convex geometry and n-dimensional methods to automatically determine endmembers for subpixel analysis (spectral unmixing). Another area of interest is the precision geocorrection and orthophotogrammetry of hyperspectral data. He is also one of the original developers of the remote sensing analysis software package ENVI, "The Environment for Visualizing Images."

Jonathan F. Huntington received the B.S. degree (with honors) from Kingston Polytechnic, University of London, London, U.K., and the Ph.D. and D.I.C. degrees from the Royal School of Mines, Imperial College of Science and Technology, University of London, in 1968 and 1974, respectively, all in geology.

He is a world-renowned research scientist in the areas of hyperspectral technology and its application to exploration geology and mining. He is currently Chief Research Scientist, Mineral Mapping Technologies, Division of Exploration and Mining, Commonwealth Scientific and Industrial Research Organisation, Sydney, Australia. His current responsibilities include development of methods to enhance and increase the geological and exploration utility of spectral data acquired in mines and the field using portable spectrometers, and remotely sensed data collected using aircraft and satellite platforms, in Australia and globally. His research, and that of his group, has defined the extent to which visible and infrared spectroscopy can be used to identify minerals, rocks, and soils routinely from drill core and rock chips, along with vegetation in the field, and from the air. He is an international authority on the spectroscopic signatures of rock forming and alteration minerals that can be used as pointers to ore-bearing environments or lead to solutions to problems in mineral processing.

Dr. Huntington was the joint winner of the 1995 Australia Prize for Science and Technology Promoting Human Welfare for "Excellence in the field of Remote Sensing."